Photoelectrochemical activity of CuO-CdS heterostructured catalyst for CO_2 reduction

IOP Conf. Series: Materials Science and Engineering **736** (2020) 042023 doi:10.1088/1757-899X/736/4/042023

Photoelectrochemical activity of CuO-CdS heterostructured catalyst for CO_2 reduction

Mostafa Tarek[1,2], Kaykobad Md. Rezaul Karim[1], Sumaya Sarmin[1,2], Huei Ruey Ong[1,3], Hamidah Abdullah[1], Chin Kui Cheng[1,2] Md. Maksudur Rahman Khan[1, 2*]

[1] Faculty of Chemical & Natural Resources Engineering; [2]Centre of Excellence for Advanced Research in Fluid Flow (CARIFF), Universiti Malaysia Pahang, 26300 Gambang, Pahang, Malaysia; [3] Faculty of Engineering and Technology, DRB-HICOM University of Automotive Malaysia, 26607 Pekan, Pahang, Malaysia.

*Corresponding author: mrkhancep@yahoo.com

Abstract. The present study explored the efficiency of a p-n heterostructured hybrid catalyst CuO-CdS to convert CO_2 selectively into methanol by photoelectrochemical (PEC) method under concurrent visible light irradiation and a bias potential -0.4 V vs. NHE. The results showed that the inclusion of CdS with CuO significantly enhanced the activity of PEC CO_2 reduction to produce methanol by facilitating the separation of photogenerated electron-hole (e^-/h^+) pairs through the p-n heterostructured architectures. The yield of methanol, the incident photon current efficiency (IPCE) and quantum efficiency (QE) in PEC CO_2 reduction were achieved 35.65 $\mu moleL^{-1}cm^{-2}$, 20.24% and 24.11%, respectively. The present work bears a new understanding into the fabrication of high- performable artificial p-n type heterostructured catalyst which is capable to function as a catalyst for photocathode for the reduction of CO_2 and remarkable improvement in methanol yield under visible light illumination.

1. Introduction

Nowadays, recycling of CO_2 via clean and environment-friendly photoelectrochemical (PEC) system to valuable fuels is a potential solution for energy demand as well as environmental emergency. In the PEC system, the concurrent flow of electrons generated by photo and electric field can boost the CO_2 reduction activity. The improvement of the catalyst activity and selectivity with higher utilization of solar energy at a lower bias potential is the main research agenda for the development of the PEC system. The bias potential in the PEC causes band bending leading to the lower electron-hole (e^-/h^+) recombination rate and oriented transfer of photogenerated electrons. In last few years a significant number of works has been reported on PEC reduction of CO_2 where the main focus was to develop photocathode with higher CO_2 reduction efficiency, selectivity and stability. In order to have an effective photocathode for the CO_2 reduction in the PEC system p-type photocathode are preferred [1]. p-type CuO, Cu_2O, InP have gained specific attention as photocathode in PEC systems due to their low band gap [2-5], favorable band positions for CO_2 reduction and H_2O oxidation and higher electron conductivity [6]. Despite having the positive properties, the activity of the catalysts is low due to the higher e^-/h^+ recombination rate. Wang et al., (2018) reported that the creation of heterostructure is an

effective way to boost up the efficiency of the reaction as well as the products selectivity in the PEC CO_2 reduction process [7]. Approaches like a combination of different types semiconductors, implementing co-catalysts and fabricating a heterojunction between two materials have been reported to heighten the photocatalytic efficiency, stability, reduce the e^-/h^+ recombination rate of the catalyst [1]. Cadmium sulfide (CdS) is a well-known n-type wide bandgap semiconductor (~2.4 eV), having higher charge separation properties and light harvesting capacity and widely used as photocatalyst for different reactions [8-10]. The position of CB of CdS is more negative than -0.61 V vs. NHE which is favourable for the reduction of CO_2 [11]. Kamimura et al., (2016) reported that the photocurrent response as well as the selectivity of the products were improved by the inclusion of n-type CdS with p-type $CuZnSnS_4$ in CO_2 reduction [12]. Although, CdS is prone to photo-corrosion [13], it is shown by some researchers that by incorporation of CdS with metal or non-metallic catalysts or fabricating heterojunctions, the stability of the catalyst can be improved [14, 15]. Xu and co-workers reported that when CdS is incorporated with $BiVO_4$ then the stability of the hybrid catalyst increased significantly [16]. Considering this, incorporation of p-type CuO with n-type CdS can be an effective strategy which has never been explored in the PEC reduction of CO_2.

The present study, a p-n type heterostructure catalyst CuO-CdS was synthesized by the ultrasound assisted wet impregnation method. The hybrid catalysts were further characterized by using X-ray diffraction (XRD), Field emission scanning electron microscopy (FESEM), Energy-dispersive X-ray spectroscopy analyzer (EDX), UV-vis spectroscopy, photoluminescence spectroscopy (PL) and Mott-Schottky analysis technique. PEC characterization was carried out using the linear sweep voltammetry (LSV) and Chronoamperometry. The as-prepared catalyst was used to fabricate photocathode and investigated in the evaluation of PEC reduction of CO_2. The liquid products were analyzed by GC-FID (6890 series GC system, Agilent Technologies Co.).

2. Experimental Study

2.1. Preparation of catalysts and electrodes

CuO was prepared with a slight modification of the conventional chemical precipitation method [17]. Firstly, 0.1M concentrate solution of copper nitrate ($Cu(NO_3)_2.3H_2O$) and copper chloride ($CuCl_2$) were prepared. Then a 0.1M solution of NaOH was gradually mixed continuous stirring (pH = 14) and black precipitates were achieved. The achieved precipitates were washed by water and ethanol up to the pH reached 7. Afterwards, the washed precipitates were centrifuged and dried for overnight at 80 °C. Finally, the powdered solid was calcined at 550 °C for 5h to obtain CuO. Chemical precipitation method was used to obtain the CdS nanoparticles with a slight modification of the method described by Devi et al., (2015) [18]. Initially, 0.1M of $CdCl_2$ and Na_2S solutions were prepared. Then the solution of $CdCl_2$ was kept under continuous starring and Na_2S solution was added dropwise in the solution of $CdCl_2$ until the yellow precipitation formed which was ripened by keeping for 2.5 h under stirring at room temperature. The particles were separated by centrifuge and washed with DI water. Finally, the obtained CdS nanoparticles were kept in the vacuum oven overnight at 50 °C. CuO-CdS hybrid catalyst was prepared by wet impregnation method. For that, as prepared CuO and CdS mixed into 100 ml of absolute ethanol at a wet ratio of 1:1. Then the mixture was ultrasonicated in a closed vial for 2 h at room temperature. After that, the mixture was again ultrasonicated while the vial was kept open at 80 °C for 3 h until the powder sample was dried. The powder sample was then grinded and dried at 80 °C using a tubular furnace under N_2 condition for 1 h. The electrodes of as-prepared catalysts were equipped with the scheme described by Karim et al., (2018) [19]. Briefly, for the preparation of the electrodes, catalyst ink was prepared by adding 0.022 g of catalyst with the mixture of 150 µL of 5 wt% Nafion and isopropanol (C_3H_8O) and then the mixture was ultrasonicated for 30 minutes. Consequently, as prepared ink was brushed on the surface of Toray carbon paper (A = 1 cm^2). For the drying of the prepared electrodes were placed into the vacuum oven for 120 minutes at 80 ˚C.

2.2. Characterization

X-ray diffraction was done for the assessment of the crystalline structure of the as-prepared catalysts by using a diffractometer (RIGAKU Miniflex II) Cu Kα radiation range 2θ=10-80° and surface morphologies were investigated by FESEM (FESEM: model JEOL JSM-5410LV, Japan). The UV−vis and PL spectra of the catalyst powders were recorded employing UV 2600, Shimadzu spectrophotometer and PerkinElmer LS55 luminescence spectrophotometer, respectively. Photoelectrochemical properties and the activity of the PEC reduction of CO_2 were carried out in a double chamber PEC cell (three-electrode configuration System) where the as-prepared electrode, Ag/AgCl and platinum foil used as the working, reference and counter electrode, respectively. The PEC cell was connected to a potentiostat (Auto lab Compact PGSTAT 204, Netherland). The photocathode and anode chamber were separated by a Nafion 117 membrane and 0.1M $NaHCO_3$ solution (pH 6.8) was used as an electrolyte in both chambers. To determine the band edges of the prepared catalyst, Mott-Schottky analysis was done at a potential -0.4 V vs. NHE under CO_2 bubbling condition (500 Hz frequency). The LSV were done in the range of 0.2 to -1.0 V potential at a scan rate of 100 mVs^{-1} in both N_2 and CO_2 bubbling conditions in saturated 0.1M $NaHCO_3$ solution. Different cut-off filters were used on the photocathode surface in the range of 470 to 730 nm during the light on condition (source: XD 300 high brightness cold light) to evaluate the photocurrent response. Light sensitivity of the as-prepared catalyst was evaluated under the CO_2 bubbling condition by the chronoamperometry analysis at -0.4 V vs. NHE. To determine the liquid product in the PEC, CO_2 was purged constantly through the cathode chamber for 4 h and the current vs time data was recorded. The liquid products were collected from the cathode chamber at different time interval and analyzed by GC-FID (6890 series GC system, Agilent Technologies Co.) using DB-Waxetr Column (Agilent Technologies).

3. Results and discussion

The morphology of the as-synthesized CuO-CdS nanostructures were visualized by FESEM. Figure 1(a) represents the FESEM images of CuO-CdS nanoparticles and the FESEM images of CuO is presented in the inset in the image which reveals that the CuO nanostructures appear sheet-like morphologies. Figure 1(a) reveals that CdS are homogeneously distributed on the CuO nanoparticles surface. XRD patterns exposed the crystallinity of the CuO and CdS nanoparticles for the as-prepared CuO-CdS and is shown in Figure 1(b). The XRD pattern of Hawleyite structured CdS reveals the distinguishable peaks at 2θ = 26.62°, 43.99° and 52.03° at the planes of (111), (220) and (311), respectively. Whereas, the 2θ value of 32.59°, 35.65°, 38.71°, 46.42°, 48.94°, 53.43°, 58.21°, 61.61°, 66.44°, 68.15°, 72.30° and 72.30° represent the plane of (110), (002), (111), (112), (202), (020), (202), (002), (113), (022), (113), (312) and (004), respectively of Tenorite structure of the CuO (DB card number 1011194). The crystal size of the as prepared CdS and CuO were calculated using Scherrer formula [20] and were found 51.06 and 64.33 nm for (002) and (111) plane, respectively. The XRD pattern of the as-prepared CuO-CdS demonstrates the peaks for both Hawleyite CdS and Tenorite CuO phase demonstrating the presence of CuO and CdS in the hybrid catalyst. The CuO-CdS diffractogram shows peaks with lower intensities than CuO and CdS which could be due to the surface of the CuO particles covered by CdS could lead crystal diffraction.

Band gap of CuO, CdS and CuO-CdS catalysts was determined from the Tauc plot presented in Figure 1(c) and was found as 1.65, 2.41 and 1.91 eV, respectively. The band gaps of CuO and CdS in the present study are in close agreement with the band gaps reported in literature for similar morphology and crystallite phases of CuO (1.7 eV) [21, 22] and CdS (2.4 eV) [23]. The band gap energy of the as-prepared CuO-CdS was modified compared to CuO and CdS and revealed that the composite material can be excited by the light with lower energy (650 nm). Further study for the optical properties of as-synthesized catalysts was analyzed by the photoluminescence spectroscopy (PL) and the emission spectra are presented in Figure 1(d). For, CdS and CuO samples exhibit an intense peak centered at 640 and 615 nm, respectively. However, the inclusion of CuO with CdS the emission spectra was significantly reduced, demonstrating a reduction in the recombination rate of e^-/h^+ which is possibly

related to the formation of oxygen vacancies in CuO and an improvement in the charge carrier separation in the composite catalyst [24]. The results demostrate that the inclusion of CuO with CdS can be an effective approach to modify the band gap and to promote the charge pair separation which may enhance the photocatalytic efficiency of the catalysts [25].

To determine the flat band potential (E_{fb}) of CdS and CuO electrodes, Mott–Schottky experiments were done. The flat band potential (E_{fb}) were calculated from the intercept of the Mott-Schottky plot and the results are presented in Figure 1(e-f) [25]. For CdS, the slope of the plot (Figure 1(e)) was found positive indicating the formation of n-type material whereas for CuO the slope was negative (Figure 1 (f)) indicating the formation of p-type material. The x-axis intercepts for CdS and CuO were found as -0.54 V and +0.92 V vs. NHE. In the case of p-type semiconductor, the E_{fb} value lies close to the VB, while the E_{fb} value lies close to the CB for the n-type semiconductor. E_{fb} value was estimated for CdS and CuO were determined as -0.56 and +0.95 V vs. NHE, respectively [25]. Consequently, the VB of CuO and CB of CdS were +0.95 V and -0.56 V, respectively which are in agreement of the literature values [26, 27]. Considering the band gap energies equation, $E_{VB(CuO)} = E_{CB(CuO)}+E_{BG(CuO)}$ and $E_{VB(CdS)} = E_{CB(CdS)}+E_{BG(CdS)}$ (where E_{BG} is the band gap of the semiconductors) [28], the CB of CuO and VB for CdS were determined and were found as -0.70 V and +1.85 V, respectively.

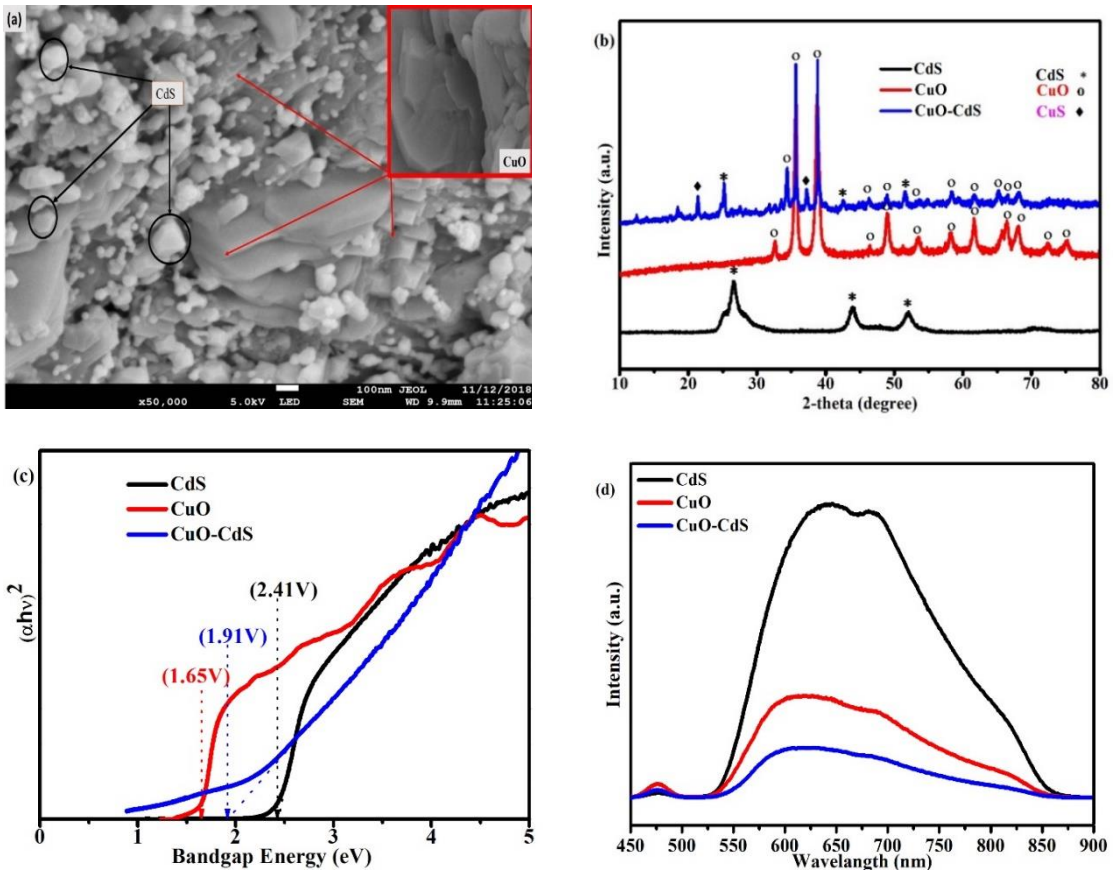

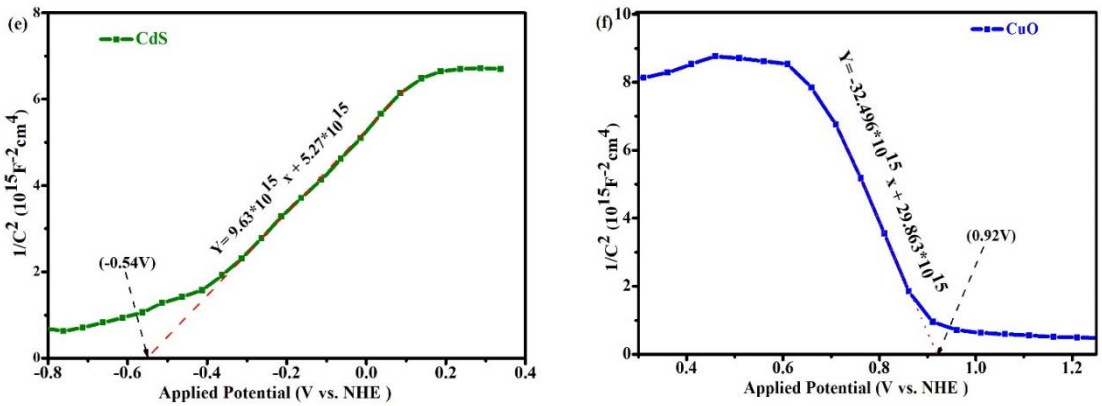

Figure 1. (a) FE-SEM image of CuO-CdS composite and inset CuO; (b) XRD pattern of as-prepared CdS, CuO and CuO-CdS; (c) Tauc plot of CdS, CuO and CuO-CdS for calculation of bandgap energy; (d) PL spectra for CdS, CuO and CuO-CdS at an excitation wavelength of 470 nm and Mott–Schottky plots of (e) CdS and (f) CuO-CdS at 0.5 kHz in 0.1M $NaHCO_3$ aqueous solution with CO_2 bubbling

The effect of applied potential on current density was recorded at a scan rate of 10 mVs^{-1} in 0.1M $NaHCO_3$ saturated with N_2 and CO_2 for the CdS, CuO and CuO-CdS electrodes in the dark (electrocatalytic) and light irradiation (photo-electrocatalytic) condition and are presented in Figure 2(a) and 2(b), respectively. In Figure 2(a) under N_2 saturation and dark condition all the electrodes showed very low reducing current suggesting the poor electrocatalytic activity for water reduction [29]. Though, under light illumination, the reducing current was slightly increased at all potential. When CO_2 was purged, a significant increase of reducing current was observed for both dark and light on the condition in Figure 2(b). The onset potential (defined as the potential when current crossed from positive to negative region) for CdS, CuO and CuO-CdS at dark conditions were found as -0.56, -0.50 and 0.054 V, respectively, while at light on conditions the onset potentials were sifted to -0.50, 0.11 and 0.135 V respectively. The results clearly demonstrated that the composite catalyst could reduce CO_2 at a more positive potential compared to the bare catalysts. Additionally, the reducing current for the CuO-CdS electrode is significantly higher than the CuO electrode at all potentials. At 1 V vs. NHE the CdS-CuO photocathode, under the light on condition, produced 22.78 mA/cm^2 compared to CuO (13.01 mA/cm^2) at the same potential. The result demonstrated that CuO-CdS achieved 2 times higher current than CuO.

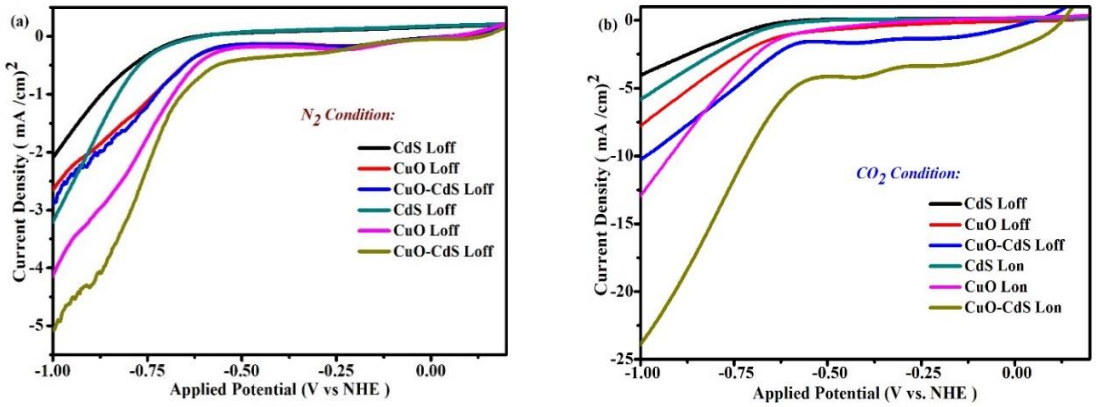

Figure 2. LSV result of CdS, CuO and CuO-CdS; (a) N_2 condition and (b) CO_2 condition at a scan rate of 10 mVs^{-1} in 0.1M $NaHCO_3$ at pH 6.8

The time-dependent photoresponse by periodically turning light on and off illumination at 470 nm at an applied potential of -0.4 V vs. NHE was performed to evaluate the photocurrent density of the photocathode and the results are shown in Figure 3(a). As CdS is an n-type semiconductor it showed an anodic current whereas CuO and CuO-CdS showed cathodic current in both light and dark condition. Figure 3(a) reveals that CuO-CdS showed ~5 times higher photocurrent (58.43 µA) compared to CuO electrode (11.02 µA). The increased photocurrent under CO_2 bubbling for CuO-CdS clearly indicates the enhanced generation of electrons, effective charge separation and efficient transfer of the charges from the bulk to the reactants which was due to the inclusion of CdS. However, no photocurrent spike was observed for CuO-CdS clearly indicates the efficient transfer of photogenerated electrons in the composite. Figure 3(b) shows the effect of applied potentials on the CuO-CdS photocathode response vs. time, which were measured under 470 nm light illumination. The photocurrent increases with the increase of applied bias (-8.35, 9.57, 20.97, 42.95, 62.22 and 83.42 µA for the bias of -0.1, -0.2, -0.3, -0.4, -0.5 and -0.6 V, respectively). A higher bias can help to separate the photogenerated e^-/h^+ pairs, leading to a higher photocurrent. While a higher current is obtained at dark condition under a higher bias, which is attributed to the more carriers release from the oxygen vacancies traps and the faster drift velocity [30]. Compared to the all bias, at -0.4 V vs. NHE the typical p-n heterostructured photocathode shows the higher photocurrent response ~53.55 µA cm^{-2}. There, the response times (the rise and decay time) are always long for a fixed bias when the light turns off. This kind of slow recuperation is accredited to the trapping states of the photogenerated carriers, which could discharge the captured e^-/h^+ slowly under an applied bias potential.

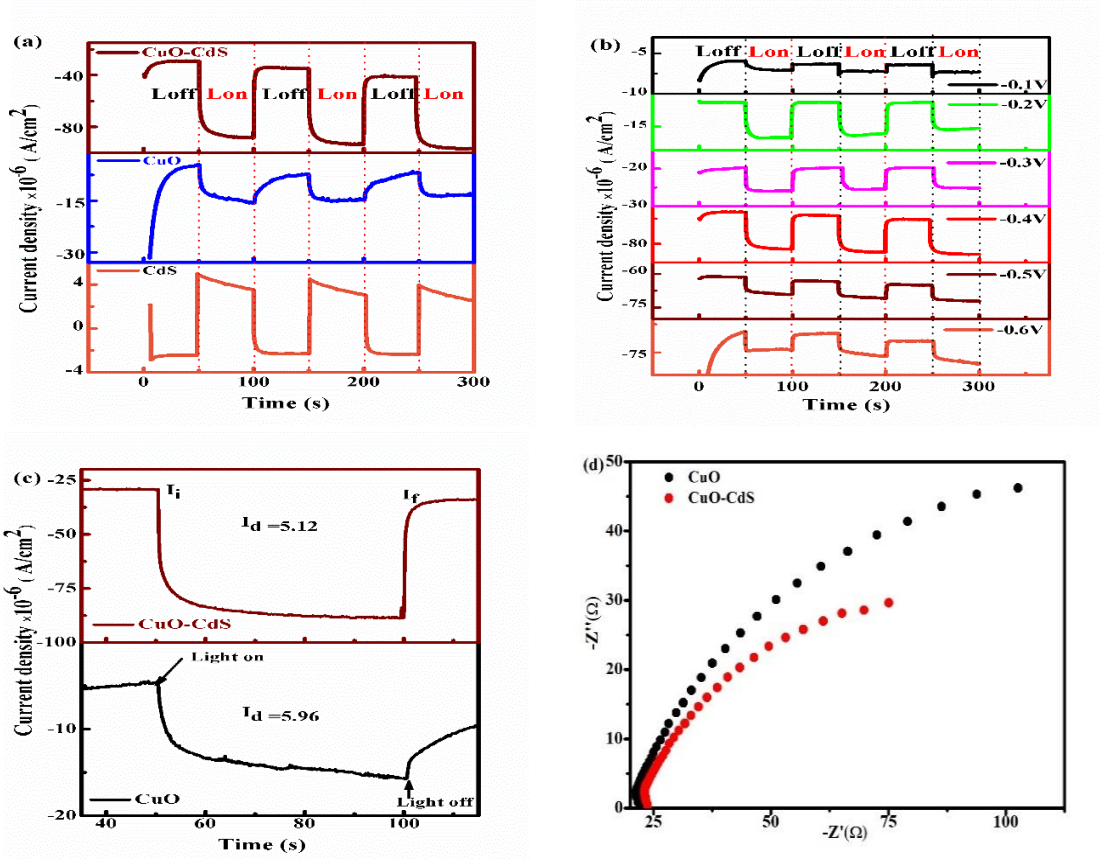

Figure 3. (a) Chronoamperometry at -0.4 V vs. NHE of CdS, CuO and CuO-CdS; (b) Chronoamperometry of CuO-CdS different potential vs. NHE; (c) current decay of CuO and CuO-CdS photocathode and (d) EIS Nyquist plots of CuO and CuO-CdS electrodes in 0.1M $NaHCO_3$

Figure 3(c) indicates that at an applied potential -0.4 V vs. NHE, the current decay (the current decay (I_d) is the variance between the initial current (I_i) and final current (I_f) of a dark/light on/dark cycle under a specific bias potential [31]) decreased for the CuO-CdS compared to the CuO photocathode which is in good agreement with the stability of the photoresponse. The charge transfer resistance of the photocatalyst was investigated through EIS. The EIS results of CuO and CuO-CdS electrodes are shown in Nyquist plot (Figure 3(d)). The semicircle of the Nyquist plot of the CuO-CdS electrode is smaller than that of the CuO electrode, which demonstrated a lower interfacial charge transfer resistance. Therefore, CuO-CdS could achieve the rapid transport of charge carriers and the effective charge separation [32] leading to higher photoreduction efficiency [33, 34].

The IPCE was calculated using the following equation:

$$\text{IPCE (\%)} = \frac{1239.7 \times \text{photocurrent genertion } (\frac{\text{mA}}{\text{cm}^2})}{\text{Wavelength of light } (\lambda \text{ in nm}) \times \text{intensity of the irradiated light } (\frac{\text{mW}}{\text{cm}^2})} \times 100 \qquad (1)$$

IPCE action spectrum of CuO-CdS is presented in Figure 4(a). The value of IPCE were found 20.24, 18.06, 14.65, 9.37 and 7.63% with an irradiation wavelength at 470, 570, 630, 690 and 730 nm, respectively. IPCE specified that CuO-CdS has the ability to absorb the visible light that can lead the e^-/h^+ generation and the charge transfer in this photocatalyst can drive the reduction of CO_2. Product distribution during the PEC reduction of CO_2 over CuO and CuO-CdS photocathode are presented in (Figure 4b). The reduction reaction is conducted for 4h under CO_2 purging condition at an applied potential -0.4 V vs. NHE. In that condition, methanol was found as a major product with the yield of 15.25 and 35.65 μmole/Lcm^2 for CuO and CuO-CdS, respectively in the liquid phase. The methanol yield was increased ~87% in CuO-CdS compared to the CuO which is in accordance with the results of LSV (Figure 2(a-b)) and Chronoamperometry (Figure 3(a)). In the gas samples insignificant amount of CO was also detected during the reduction reaction (0.35 and 2.7 $\mu molL^{-1}cm^{-2}$ for CuO and CuO-CdS, respectively). However, 0.45 $\mu molL^{-1}cm^{-2}$ H_2 was found for CuO-CdS photocathode only. Finally, CO_2 reduction was accomplished for 4h over CuO-CdS photocathode in the PC, EC and PEC system. Methanol was the sole-product in the liquid phase and the achieved methanol yields are shown in (Figure 4c). EC showed lower methanol yield 9.25 $\mu molL^{-1}cm^{-2}$ compared to the PC 17.1 $\mu molL^{-1}cm^{-2}$ whereas, in the PEC system, the yield increased significantly. The QE and the FE in the PEC system were calculated by using the method described in Karim et al., (2018) [35]. It was found that the QE was increased from 10.34% (for CuO) to 24.11% (for CuO-CdS) which is due to the efficient charge separation. The FE was increased from 43% (for CuO) to 86% (CuO-CdS) at an applied potential of -0.4 V vs. NHE for the reduction of CO_2 in PEC due to the inclusion of CdS with CuO.

The mechanism of enhancement of PEC CO_2 reduction due to the transfer of photogenerated electrons from CuO to CdS in CuO-CdS heterostructure is illustrated in (Figure 4(d)). Due to the lower band gap, CuO could produce the photogenerated electron which could easily be transferred to the CB of CdS, as its CB is less negative compared to CuO where the CO_2 reduction could take place. On the other hand, the VB level of CdS is lower than the CuO and as a result, the photogenerated holes in the VB of CdS can easily be transferred to the VB of CuO which can act as the oxidation site. Hence, the separation, as well as the migration of photogenerated electrons carriers, could be raised by the internal photogenerated electric field resulted in less barrier. Consequently, the possibility of e^-/h^+ recombination can be decreased. Additionally, Jiang et al.,(2001) reported that a suitable bias potential to the photoelectrode promoted the separation of charge carriers within the semiconductor electrode which played the crucial role to enhance the efficiency of reduction activity at the semiconductor/electrolyte interface [36]. Therefor, the applied potential -0.4 V vs. NHE could also effectively separate the e^-/h^+, which is an advantage for the PEC reduction of CO_2. Methanol was found as the main product suggesting the $6e^-$ transfer reaction of CO_2. CuO has an acceptor level and capable to trap electrons from the VB [37]. Due to this fact, it can be predicted that the number of holes in CuO is much bigger than that of electrons. The reverse is true for the n-type CdS where the electron density is higher in CB. Therefore, it can be speculated that the CO_2 reduction could occur on the CB of CdS and the p-type CuO VB is more suitable for the oxidation of water.

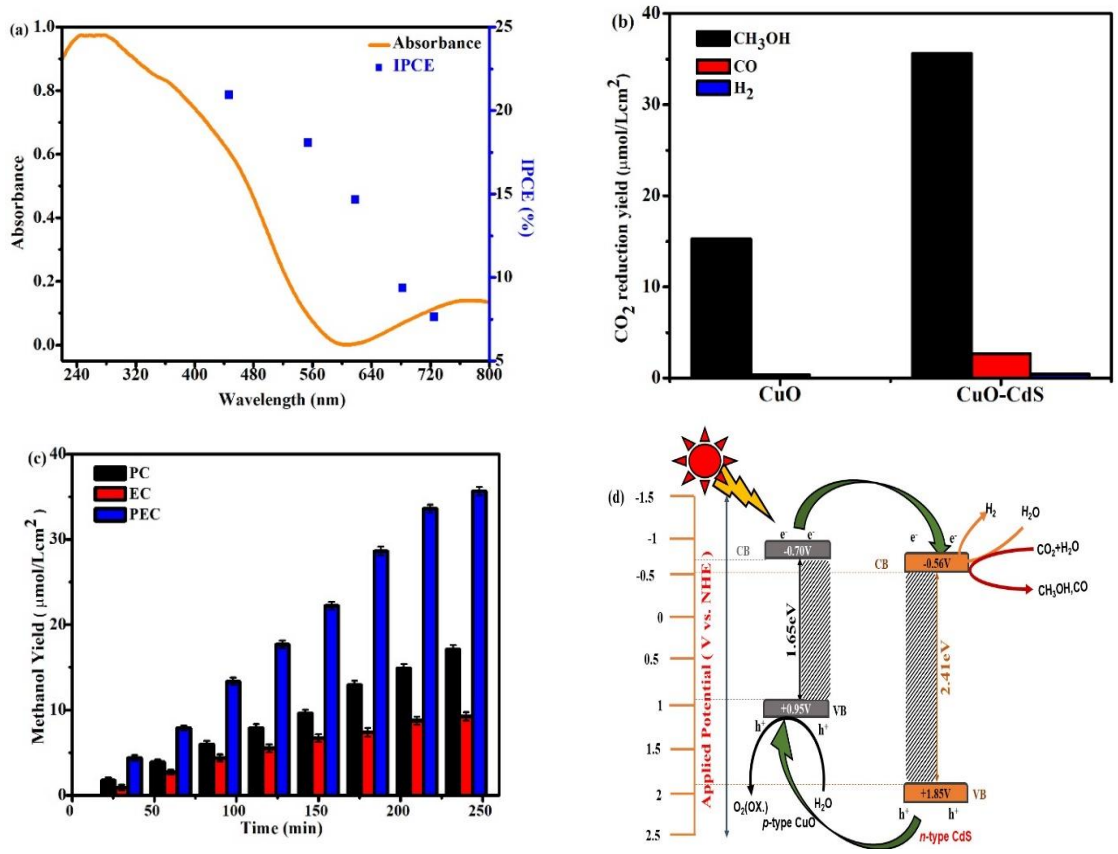

Figure 4. (a) UV-vis spectra of CuO-CdS photocathode along with IPCE in several wavelengths (470-730 nm); (b) Product yield for CuO and CuO-CdS in PEC reduction of CO_2; (c) Methanol yield over CuO-CdS at -0.4 V vs. NHE potential in 0.1M $NaHCO_3$ solution under 470 nm wavelength light irradiation and (d) Proposed mechanism for photoelectrocatalytic reduction of CO_2 over CuO-CdS photocathode surface

4. Conclusion

The present work demonstrated enormous prospective for the heterostructure of CuO-CdS in CO_2 conversion in aqueous phase producing selectively methanol. The inclusion of CuO with CdS can effectively promote the separation of photogenerated carriers and provide more active sites for CO_2 reduction. Heterostructured CuO-CdS possessed 20.24 % IPCE at 470 nm which clearly indicates the proficiency of CuO-CdS photocathode in absorbing the visible light leading to 35.65 $\mu moleL^{-1}cm^{-2}$ methanol yield in 0.1M $NaHCO_3$ aqueous solution at an applied potential of -0.4 V vs. NHE. The CuO-CdS photocathode achieved 86 and 24.11 % of FE and QE, respectively. Overall, these results indicate that p-n type of CuO-CdS hybrid nanocomposites is capable of producing value-added chemicals from CO_2 in PEC system.

Acknowledgement
We are thankful to Universiti Malaysia Pahang (RDU 1603127 and Flagship Strategic Leap 3 Grant RDU 172202) and SABIC, King Abdulaziz University (UIC151501) for supporting the research.

References

[1] Kalamaras E, Maroto-Valer M M, Shao M, Xuan J and Wang H J C T 2018 Solar carbon fuel via photoelectrochemistry **317** 56-75
[2] Ghadimkhani G, de Tacconi N R, Chanmanee W, Janaky C and Rajeshwar K J C C 2013 Efficient solar photoelectrosynthesis of methanol from carbon dioxide using hybrid CuO–Cu_2O semiconductor nanorod arrays **49** 1297-9
[3] Li P, Xu J, Jing H, Wu C, Peng H, Lu J and Yin H J A C B E 2014 Wedged N-doped CuO with more negative conductive band and lower overpotential for high efficiency photoelectric converting CO_2 to methanol **156** 134-40
[4] Li C W and Kanan M W J J o t A C S 2012 CO_2 reduction at low overpotential on Cu electrodes resulting from the reduction of thick Cu_2O films **134** 7231-4
[5] Ohya S, Kaneco S, Katsumata H, Suzuki T and Ohta K J C T 2009 Electrochemical reduction of CO_2 in methanol with aid of CuO and Cu_2O **148** 329-34
[6] Rajeshwar K, de Tacconi N R, Ghadimkhani G, Chanmanee W and Janáky C J C 2013 Tailoring copper oxide semiconductor nanorod arrays for photoelectrochemical reduction of carbon dioxide to methanol **14** 2251-9
[7] Wang P, Wang S, Wang H, Wu Z, Wang L J P and Characterization P S 2018 Recent Progress on Photo- Electrocatalytic Reduction of Carbon Dioxide **35** 1700371
[8] Nozik A J P E L-d S and Nanostructures 2002 Quantum dot solar cells **14** 115-20
[9] Shen Q, Zhao X, Zhou S, Hou W and Zhu J-J J T J o P C C 2011 ZnO/CdS hierarchical nanospheres for photoelectrochemical sensing of Cu^{2+} **115** 17958-64
[10] Guo X, Chen C, Song W, Wang X, Di W and Qin W J J o M C A C 2014 CdS embedded TiO_2 hybrid nanospheres for visible light photocatalysis **387** 1-6
[11] Zhao G, Huang X, Wang X and Wang X J J o M C A 2017 Progress in catalyst exploration for heterogeneous CO_2 reduction and utilization: A critical review **5** 21625-49
[12] Kamimura S, Sasaki Y, Kanaya M, Tsubota T and Ohno T 2016 Improvement of selectivity for CO_2 reduction by using Cu_2ZnSnS_4 electrodes modified with different buffer layers (CdS and In_2S_3) under visible light irradiation RSC Advances **6** 112594-601
[13] Tang Y, Hu X and Liu C J P C C P 2014 Perfect inhibition of CdS photocorrosion by graphene sheltering engineering on TiO_2 nanotube array for highly stable photocatalytic activity **16** 25321-9
[14] Yang Y, Zhang Y, Fang Z, Zhang L, Zheng Z, Wang Z, Feng W, Weng S, Zhang S, Liu P J A a m and interfaces 2017 Simultaneous realization of enhanced photoactivity and promoted photostability by multilayered MoS_2 coating on CdS nanowire structure via compact coating methodology **9** 6950-8
[15] Hou J, Yang C, Wang Z, Jiao S and Zhu H J R A 2012 Hydrothermal synthesis of CdS/$CdLa_2S_4$ heterostructures for efficient visible-light-driven photocatalytic hydrogen production **2** 10330-6
[16] Fang S, Xue S, Wang C, Wang G, Wang X, Liang Q, Li Z and Xu S J C I 2016 Fabrication and characterization of CdS/$BiVO_4$ nanocomposites with efficient visible light driven photocatalytic activities **42** 4421-8
[17] Phiwdang K, Suphankij S, Mekprasart W and Pecharapa W 2013 Synthesis of CuO nanoparticles by precipitation method using different precursors Energy Procedia **34** 740-5
[18] Devi R A, Latha M, Velumani S, Oza G, Reyes-Figueroa P, Rohini M, Becerril-Juarez I, Lee J-H, Yi J J o n and nanotechnology 2015 Synthesis and characterization of cadmium sulfide nanoparticles by chemical precipitation method Journal of nanoscience nanotechnology **15** 8434-9
[19] Rezaul Karim K M, Tarek M, Ong H R, Abdullah H, Yousuf A, Cheng C K and Khan M M R 2018 Photoelectrocatalytic Reduction of Carbon Dioxide to Methanol using $CuFe_2O_4$ Modified with Graphene Oxide under Visible Light Irradiation Industrial Engineering Chemistry Research

[20] Uddin M R, Khan M R, Rahman M W, Yousuf A, Cheng C K J R K, Mechanisms and Catalysis 2015 Photocatalytic reduction of CO_2 into methanol over $CuFe_2O_4/TiO_2$ under visible light irradiation **116** 589-604
[21] Basnet P 2015 Metal oxide photocatalytic nanostructures fabricated by dynamic shadowing growth. University of Georgia)
[22] Yang J, Li Z, Zhao W, Zhao C, Wang Y and Liu X J M L 2014 Controllable synthesis of Ag–CuO composite nanosheets with enhanced photocatalytic property **120** 16-9
[23] Shen Q, Zhao X, Zhou S, Hou W and Zhu J-J 2011 ZnO/CdS hierarchical nanospheres for photoelectrochemical sensing of Cu^{2+} The Journal of Physical Chemistry C **115** 17958-64
[24] Khan M M R, Uddin M R, Abdullah H, Karim K M R, Yousuf A, Cheng C K, Ong H R J I J o C, Molecular, Nuclear, Materials and Engineering M 2016 Preparation and Characterization of $CuFe_2O_4/TiO_2$ Photocatalyst for the Conversion of CO_2 into Methanol under Visible Light **10** 1165-72
[25] Kamimura S, Murakami N, Tsubota T and Ohno T 2015 Fabrication and characterization of a p-type $Cu_3Nb_2O_8$ photocathode toward photoelectrochemical reduction of carbon dioxide Applied Catalysis B: Environmental **174** 471-6
[26] Madhusudan P, Zhang J, Cheng B and Yu J 2015 Fabrication of $CdMoO_4$@ CdS core–shell hollow superstructures as high performance visible-light driven photocatalysts Physical Chemistry Chemical Physics **17** 15339-47
[27] Wang P, Wang S, Wang H, Wu Z and Wang L 2018 Recent Progress on Photo- Electrocatalytic Reduction of Carbon Dioxide Particle Particle Systems Characterization **35** 1700371
[28] Dong H, Chen G, Sun J, Feng Y, Li C, Xiong G and Lv C 2014 Highly-effective photocatalytic properties and interfacial transfer efficiencies of charge carriers for the novel Ag_2CO_3/AgX heterojunctions achieved by surface modification Dalton Transactions **43** 7282-9
[29] de Brito J F, Araujo A R, Rajeshwar K and Zanoni M V B J C e j 2015 Photoelectrochemical reduction of CO_2 on Cu/Cu_2O films: Product distribution and pH effects **264** 302-9
[30] Guo D, Shi H, Qian Y, Lv M, Li P, Su Y, Liu Q, Chen K, Wang S, Cui C J S S and Technology 2017 Fabrication of β-Ga_2O_3/ZnO heterojunction for solar-blind deep ultraviolet photodetection **32** 03LT1
[31] Tamirat A G, Su W-N, Dubale A A, Chen H-M and Hwang B-J J J o M C A 2015 Photoelectrochemical water splitting at low applied potential using a NiOOH coated codoped (Sn, Zr) α-Fe_2O_3 photoanode **3** 5949-61
[32] He B-L, Dong B and Li H-L J E C 2007 Preparation and electrochemical properties of Ag-modified TiO_2 nanotube anode material for lithium–ion battery **9** 425-30
[33] Park Y, Kang S-H and Choi W J P C C P 2011 Exfoliated and reorganized graphite oxide on titania nanoparticles as an auxiliary co-catalyst for photocatalytic solar conversion **13** 9425-31
[34] Li X, Liu A, Chu D, Zhang C, Du Y, Huang J and Yang P J C 2018 High performance of manganese porphyrin sensitized p-type $CuFe_2O_4$ photocathode for solar water splitting to produce hydrogen in a tandem photoelectrochemical cell **8** 108
[35] Karim K M R, Ong H R, Abdullah H, Yousuf A, Cheng C K and Khan M M R 2018 Photoelectrochemical reduction of carbon dioxide to methanol on p-type $CuFe_2O_4$ under visible light irradiation International Journal of Hydrogen Energy **43** 18185-93
[36] Jiang D, Zhao H, Jia Z, Cao J and John R 2001 Photoelectrochemical behaviour of methanol oxidation at nanoporous TiO_2 film electrodes Journal of Photochemistry Photobiology A: Chemistry **144** 197-204
[37] Luo J, Dong G, Zhu Y, Yang Z and Wang C 2017 Switching of semiconducting behavior from n-type to p-type induced high photocatalytic NO removal activity in g-C_3N_4 Applied Catalysis B: Environmental **214** 46-56